Atom Indonesia

Journal homepage: http://atomindonesia.brin.go.id

Application of Sub-Miniature Fission Chamber Neutron Detector for Neutron Flux Measurement at the RSG-GAS Reactor: Foil Activation Benchmarking

R. Gusman[1,2], A. Agung[1*], R. M. Subekti[2], F. N. Iswahyudi[2], F. Susanti[2], S. Pinem[3]

[1]*Department of Nuclear Engineering and Engineering Physics – Universitas Gadjah Mada, Yogyakarta, 55281, Indonesia*
[2]*Directorate of Nuclear Facility Management – National Research and Innovation Agency, Serpong 15314, Indonesia*
[3]*Nuclear Reactor Technology Research Center – National Research and Innovation Agency, Serpong 15314, Indonesia*

ARTICLE INFO

Article history:
Received 4 August 2025
Received in revised form 15 October 2025
Accepted 20 October 2025

Keywords:

Sub-miniature fission chamber
Thermal neutron flux
Gold foil activation
RSG-GAS reactor

ABSTRACT

Accurate neutron flux measurement is essential for reactor characterization and utilization. At the RSG-GAS reactor, previous flux measurements relied on the foil activation method. While this method provides high accuracy, it lacks real-time capability due to its requirement for irradiation, post-irradiation cooling, and subsequent gamma spectroscopy for activity assessment. Direct online measurements of thermal neutron flux in the RSG-GAS reactor irradiation positions were performed using a Sub-Miniature Fission Chamber (SMFC) detector, where the flux was determined from the detector's output current proportional to fission events. This approach offers a viable alternative to the conventional foil activation technique by eliminating its time-consuming process and multiple uncertainty sources. After applying a correction factor obtained from gold foil activation reference measurements and the combined measurement uncertainty was quantified as ± 4.0%, results showed an axial flux distribution peaking at 200 mm height from the bottom of the core with maximum values of 4.997 x 10^{12} ± 0.199 x 10^{12} n/cm².s at central iradiation position (CIP E7), 6.212 x 10^{12} ± 0.248 x 10^{12} n/cm².s at iradiation position (IP B6), and 2.096 x 10^{12} ± 0.083x10^{12} n/cm².s at reflector element with plug (BS+ A2) under 200 kW operation. Radial mapping at 600 mm height from the bottom of the core revealed a maximum flux of 1.230 x 10^{12} ± 0.049 x 10^{12} n/cm².s at IP (G7). These results demonstrate that the Sub-Miniature Fission Chamber (SMFC) enables real-time neutron flux monitoring and provides a viable alternative to the conventional foil activation technique.

INTRODUCTION

The G.A. Siwabessy Multipurpose Reactor (RSG-GAS) is a 30 MW thermal Material Testing Reactor (MTR) utilizing low-enriched uranium silicide fuel (U_3Si_2-Al, 19.75% enrichment, 2.96 gU/cm^3 uranium density). Under full-power operation, RSG-GAS generates a nominal average thermal neutron flux of ~2.00 x 10^{14} n/cm².s in the core region, making it suitable for various nuclear research applications [1].

In research reactors, precise neutron flux measurements are essential for supporting target irradiation processes and ensuring accurate experimental conditions within the reactor core [2]. Current neutron flux monitoring in the RSG-GAS reactor employs the foil activation method utilizing gold (Au) foils. Following irradiation, the induced activity of the gold foils is quantified using a gamma-ray spectrometer equipped wit a Multi-Channel Analyzer (MCA), where the measured activity directly correlates with the incident neutron flux [3]. The conventional foil activation method requires substantial processing time, involving sequential steps of sample preparation, irradiation at target positions, gamma-ray counting, and post-irradiation analysis to calculate neutron flux values.

*Corresponding author.
E-mail address: a_agung@ugm.ac.id
DOI: https://doi.org/10.55981/aij.2026.1768

Contemporary research reactors increasingly employ direct neutron flux measurement techniques utilizing specialized detectors, including fission chambers and Self-Powered Neutron Detectors (SPNDs), which provide real-time monitoring capabilities [4-7]. Several studies have developed and characterized micro-fission chambers, proposing theoretical models for sub-miniature variants (e.g., ~1.5 mm diameter) that address in-core detection [8]. Complementary research has explored high-sensitivity U-233–based fission counters and proposed miniature fission chamber designs for in-core reactor applications [9]. More recently, Monte Carlo simulations, validated via irradiation experiments, have been employed to assess the neutron sensitivity of micro-fission chambers, demonstrating strong agreement between simulated and empirical results [10]. Despite these advancements, the lack of comprehensive validation against the foil activation method still challenges the fission chamber performance, including comparing its performance to the existing studies that have been conducted in other reactors with different neutron spectra.

A fission chamber detector enables direct neutron flux measurements in research reactor irradiation facilities by correlating the detector output current with the incident neutron flux. As a relative measurement method, it requires periodic calibration against a foil activation method. Nevertheless, no prior study has systematically validated sub-miniature fission chamber measurements through direct comparison with the foil activation technique in the RSG-GAS reactor. The objective of this study, thermal neutron flux measurements in the RSG-GAS reactor irradiation facilities were performed using a Sub-Miniature Fission Chamber (SMFC), with verification provided by benchmarking to the gold foil activation method. This direct measurement approach offers significant improvements in efficiency, facilitating more streamlined neutron flux mapping and enhancing irradiation process management in the RSG-GAS reactor core.

THEORY

Description of RSG GAS reactor

The RSG-GAS reactor, an open-pool type research reactor, attained initial criticality on 29 July 1987 with a core configuration of 12 Fuel Elements (FEs) and 6 Control Elements (CEs). Located at the B.J. Habibie Science and Technology Area (KST) within the Puspiptek Area, South Tangerang, Indonesia, the reactor utilizes low-enriched uranium (LEU, 19.75% ^{235}U) fuel. Originally employing uranium oxide (U_3O_8-Al) fuel with a uranium density of 2.96 gU/cm^3, the reactor was subsequently converted to uranium silicide (U_3Si_2-Al) fuel while maintaining the same uranium density. The reactor's primary systems include light water serving dual functions as coolant and moderator, complemented by beryllium neutron reflectors [11-12]. The RSG-GAS reactor operates at a nominal thermal power output of 30 MWth, generating characteristic thermal neutron flux on the order of 10^{14} n/cm^2.s in the core and 10^{13} n/cm^2.s in the reflector [3].

The RSG-GAS reactor core configuration comprises 40 FEs and 8 CEs, containing 21 and 15 fuel plates per element, respectively. The control elements incorporate neutron-absorbing Ag-In-Cd alloy control rods (18 wt% Ag, 15 wt% In, 5 wt% Cd) for reactivity regulation. Table 1 summarizes the principal reactor design specifications and operating parameters [13]. The geometric specifications of both FEs and CEs, along with the equilibrium core configuration, are illustrated in Figs. 1 and 2, respectively.

Table 1. Main data RSG-GAS reactor design parameters [13].

Parameters	Specification
Type of fuel	U_3Si_2-Al
Enrichment, %	19.75
Uranium density in meat, g/cm^3	2.96
Cladding material	AlMg2
Type of absorber	Fork type
Material absorber	Ag-In-Cd
Absorber thickness, mm	3.38
Absorber cladding material	Steels
Active length, cm	60
Number of standard fuel elements at typical working core	40
Fuel plates per standard fuel element	21
Number of control fuel elements at typical working core	8
Fuel plates per control fuel element	15
Core thermal power, MW	30
Effective flow rate for fuel cooling plates, kg/s	618
Nominal inlet temperature, °C	40.5
Average temperature increases in reactor core, K	10.7
Average outlet temperature in reactor core, °C	50.57
Outlet maximum temperature of hot channel, °C	75.3
Surface area of fuel plates, m^2	72.29

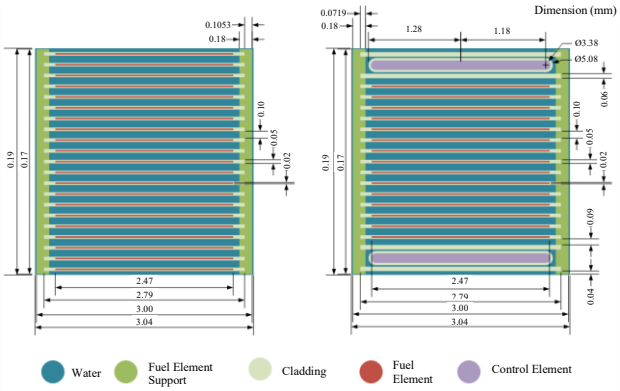

Fig. 1. Fuel element (left) and control element (right) of RSG-GAS (units in mm) [14].

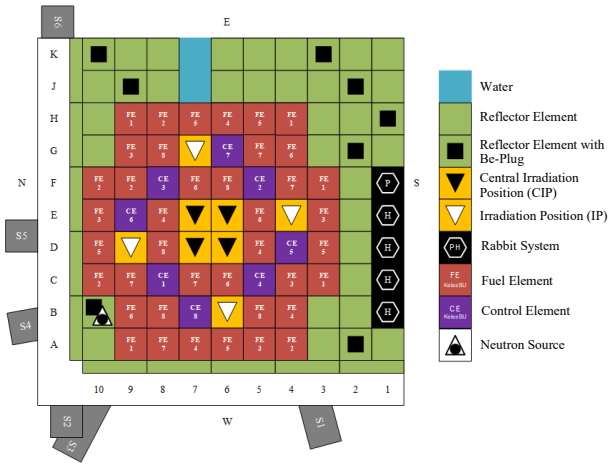

Fig. 2. Equilibrium core configuration of the RSG-GAS reactor [14].

The RSG-GAS reactor provides diverse neutron irradiation capabilities through its specialized facilities: the Central Irradiation Position (CIP) for high-flux applications, Irradiation Positions (IPs) for material testing, radial neutron beam tubes for experimental beamline access, rabbit system for rapid sample transfer, the Power Ramp Test Facility (PRTF) for fuel performance studies, and the reflector element with plug irradiation facility (BS+) for specialized experiments. These integrated irradiation facilities enable concurrent multidisciplinary research, from radioisotope production to neutron scattering studies [15-16]. The RSG-GAS irradiation facilities support multidisciplinary applications across advanced material testing, industrial processing, and academic research. Primary utilization focuses on research, education, and training programs, while dedicated systems enable radioisotope production for medical diagnostic, industrial radiography, gemstone coloration, and neutron activation analysis.

Fission chamber detector

The fission chamber detector, a specialized variant of the ionization chamber, incorporates fissile material coatings to enable neutron-sensitive measurements. This instrument provides real-time monitoring of key reactor parameters, including thermal power output, neutron flux distribution, fuel burnup fraction, and other related applications [17-18]. The fission chamber detector features a cylindrical geometry comprising two concentric electrodes (anode and cathode), with the anode surface typically coated with a thin layer of fissile material such as ^{235}U (Uranium-235). The inter-electrode volume is filled with pressurized noble gas chosen for its chemical inertness and stable ionization properties under reactor conditions. Recent advances in fission chamber technology have focused on optimized detector geometries for enhanced spatial resolution, advanced fissile coatings for improved neutron sensitivity, and real-time flux mapping algorithms for high-accuracy power monitoring applications [19-22].

Figure 3 presents the schematic diagram of a fission chamber detector, operating through thermal neutron-induced fission reactions. The detection mechanism initiates when thermal neutrons (E < 0.025 eV) are absorbed by ^{235}U nuclei n the coating layer, inducing nuclear fission. This process generates two high-energy fission fragments (~80-100 MeV total) that ionize the surrounding argon gas, producing measurable charge pulses proportional to the incident neutron flux [23].

Gas-filled detectors operate across three characteristic voltage-dependent regions (Fig. 4). The recombination region (typically < 50 V), where ion pairs rapidly recombine due to insufficient electric field strength. The saturation region (~100-300 V), where a stable current plateau forms as ~95% of primary ion pairs are collected with negligible recombination. The proportional region (~300-1000 V), where avalanche multiplication yields gas gain factors of 10^3-10^4 through secondary ionization, enabling sensitive neutron detection while maintaining linearity between ionization events and output signals.

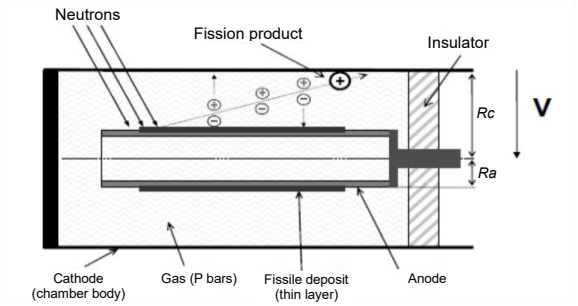

Fig. 3. Schematic diagram of a typical fission chamber detector [23].

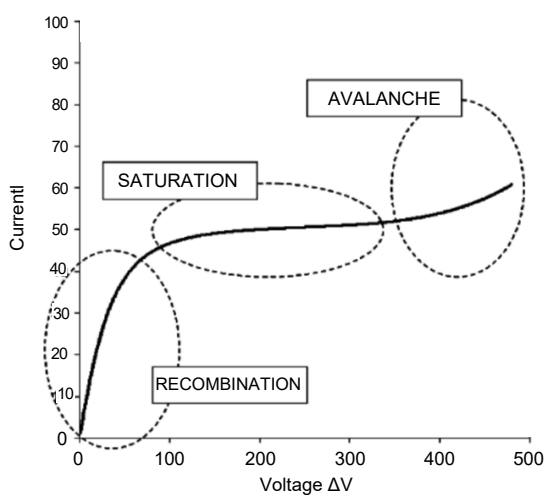

Fig. 4. Gas-filled detector curve [24].

The output current of a fission chamber detector in current-mode operation is governed by the coupled Eqs. (1-5) [24].

$$I = I_{rec} + I_{sat} + I_{sec} \quad (1)$$

$$I_{rec} = -e \iiint_V kn_e n_a \, dV \quad (2)$$

$$I_{sat} = e \iiint_V N \, dV \quad (3)$$

$$I_{sec} = e \iiint_V a(E) n_e v_e \, dV \quad (4)$$

$$I = e \iiint_V (N - kn_e n_a + a(E) n_e v_e) dV \quad (5)$$

The output current of the fission chamber detector in current-mode operation is governed by the V parameters corresponds to the filled gas volume between electrodes, n_e and n_a corresponds to electron and ion densities, respectively, E corresponds to applied electric field, N corresponds to ion pair density generated by fission products per unit time, v_e corresponds to electron drift velocity, k corresponds to volumetric recombination coefficient, and α corresponds to Townsend ionization coefficient, representing secondary electron generation per unit path length). The detector characteristics are further described by three current components: I_{sat} (saturation current, determined by detector geometry and neutron flux), I_{rec} (recombination current loss), and I_{sec} (secondary ionization gain). In this study, the detector was operated in the saturation region (current mode), where the output current becomes independent of applied voltage and the measured current depends solely on the incident neutron flux. Equation (1) simplifies to reflect only the primary ionization density (N). So, the detector output current is only measured in the saturation region.

Sub-Minature Fission Chamber (SMFC)

The Sub-Miniature Fission Chamber (SMFC) is a compact neutron detector developed by Photonis (France) under proprietary technology licensed from the French Alternative Energies and Atomic Energy Commission (CEA) [7]. This study utilized the SMFC CFUZ53 detector, a miniature fission chamber with 1.5 mm outer diameter containing 10 µg of 90%-enriched ^{235}U and argon fill gas (110 kPa). The detector exhibits a thermal neutron sensitivity of 5 x 10^{-18} A/n.cm^{-2}.s^{-1} and operates in current mode for flux measurements up to 1 x 10^{14}n/cm^2.s.

Figure 5 illustrates the SMFC CFUZ53's schematic configuration and dimensions. The SMFC CFUZ53 detector's properties, including nuclear, electrical, and mechanical, are summarized in Table 2.

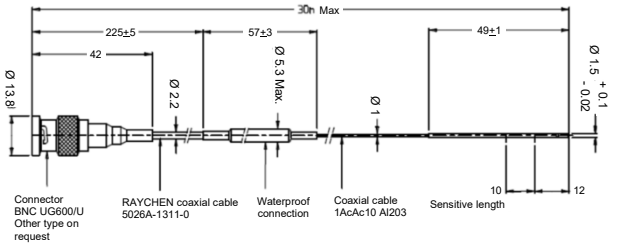

Fig. 5. Schematic of SMFC CFUZ53.

Table 2. Specification SMFC CFUZ53.

Nuclear Properties			
Sensitivity to thermal neutrons in current mode		5 x 10^{-18}	A/n.cm^{-2}.s^{-1}
Neutron flux range in current mode		2 x 10^{11}/10^{14}	n.cm^{-2}.s^{-1}
Gamma sensitivity		7 x 10^{-13}	A/Gy.h^{-1}
Exposure limits	Thermal neutron	max 1.5 x 10^{20}	n.cm^{-2}
	Gamma expossure	max 10^{19}	Gy
	Gamma dose rate	max 10^{7}	Gy.h^{-1}
Electrical Properties			
Insulating resistance at 150 VDC	at 20ºC	Min 10^{12}	Ohm
	at 350ºC	Min 10^{8}	Ohm
Operating voltage	Nominal up to 350ºC	100	VDC
	Maximum at 20ºC	150	VDC
	Limit with no radiation	400	VDC
Cable capacitance		280	pF/m
Line resistance		1.8	Ohm.m
Mechanical and Physical Properties			
Detector	Case, electrodes	Stainless steel (Co < 0.05%)	
	Insulators	Al_2O_3	
	Sensitive layer	U > 90% enriched in ^{235}U	
Cable	Filling gas	Argon at 110kPa	
	Type	Coaxial	
	Insulator	Al_2O_3	
	Curvature radius	min 20mm	
Connector	Type	BNC	
	Insulator	PTFE	

Counting system

The Keithley 2450 Source Measure Unit (SMU), as shown in Fig. 6, was employed as a precision source meter, capable of both sourcing DC voltage (20 mVDC – 200 VDC) to the detector and measuring current (10 nA – 1 A) from the detector. Configured to supply a stable 100 VDC bias to the fission chamber detector while simultaneously measuring its output current in current mode, the instrument's four-quadrant operation and wide dynamic range ensured optimal performance for the SMFC CFUZ53's neutron flux measurements.

Fig. 6. Keithley 2450SMU.

Gold foil activation

Gold foil activation is an absolute method for measuring neutron flux in a nuclear reactor. The principle of this method is based on the interaction between neutrons and the material of the activation foil, enabling the measurement of neutron distribution within the reactor core [25]. The thermal neutron flux using this method is determined from the measured saturation activity per nucleus of a foil irradiated over a specific period. The activity of the foil is proportional to the neutron flux, taking into account the irradiation duration. Since the gold foil is activated in a neutron flux field with a broad energy spectrum, the resulting activity in the foil is caused by neutrons of all energy levels. To determine the thermal neutron flux (E < 0.5 eV), one of the gold foils must be wrapped in cadmium. Cadmium absorbs thermal neutrons, allowing for the separation of thermal and epithermal (or fast) neutron contributions. Therefore, to measure the thermal neutron flux, used following Eq. (6) [26].

$$\phi_{th} = \frac{A_r A}{m N_o \sigma_{th} (1-e^{-\lambda t_i}) e^{-\lambda t_d}} \quad (6)$$

where,

ϕ_{th} = thermal neutron flux (n/cm^2.s)
A_r = atom relative mass (g/mol)
A = saturation activity (Bq)
m = foil mass (g)
N_o = Avogadro number (atom/mol)
σ_{th} = thermal cross section (cm^2)
λ = decay constant (1/s)
t_d = delay time (s)
t_i = irradiation time (s)

METHODOLOGY

Gold foil activation neutron flux measurement method

Thermal neutron flux measurements were conducted using the foil activation method with gold-aluminum (Au-Al) alloy foils. The foils, encapsulated in separate aluminum (Al) and cadmium (Cd) coverings, were irradiated for 30 minutes at a reactor power of 200 kW within the reactor's irradiation facilities. The foils precisely certified composition and dimensions, as provided by the manufacturer, enabled absolute flux determination, consistent with IAEA technical reports [27]. Following irradiation, the foils underwent a cooling period prior to activity measurement using a high-purity germanium (HPGe) gamma spectrometer system. The spectrometer was calibrated with a suite of standard gamma sources (^{152}Eu) to ensure energy and efficiency accuracy; its detailed specifications are provided in Table 3 and Fig. 7. The resulting activity data were used to calculate the thermal neutron flux according to Eq. (6), which incorporates the number of target atoms, relevant reaction cross-section, irradiation time, and cooling duration.

Table 3. Gamma-ray spectrometry system.

Parameters	Specification
Detector	HPGe, tipe-p
High voltage supply	+ 2.5 kV
Amplifier	Canberra 2020
Coarse gain	100
Fine gain	11.4
Shaping time	4 ms
MCA	Canberra S35+
Gain	4K, 1 half
Lower level	0.10

Fig. 7. Gamma-ray spectrometry system.

Fission chamber neutron flux measurement method

Neutron flux mapping was performed using a custom-designed guide tube system to position the SMFC CFUZ53 detector within the reactor core. The aluminum alloy (AlMg3) guide tube (18 mm OD, 3 mm wall thickness; Fig. 8) serves two critical functions: precise detector positioning for axial/radial flux scans, while also protecting the detector and its cabling from the reactor coolant. AlMg3 alloy was selected for its optimal combination of mechanical strength (yield strength: 100-150 MPa), neutron transparency (low activation cross-section), and corrosion resistance in aqueous environments.

Neutron flux measurements in the RSG-GAS irradiation facilities were performed by inserting the SMFC CFUZ53 detector into the aluminum guide tube and positioning it at target locations (Fig. 9), with the detector connected to a Keithley 2450 Source Measure Unit (SMU) operating at 100 VDC bias to record output currents. The measurements were conducted under low-power reactor conditions (200 kW, natural convection cooling) to ensure thermal-hydraulic stability.

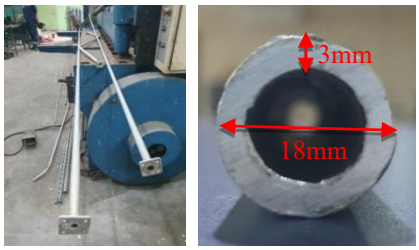

Fig. 8. Detector guide tube.

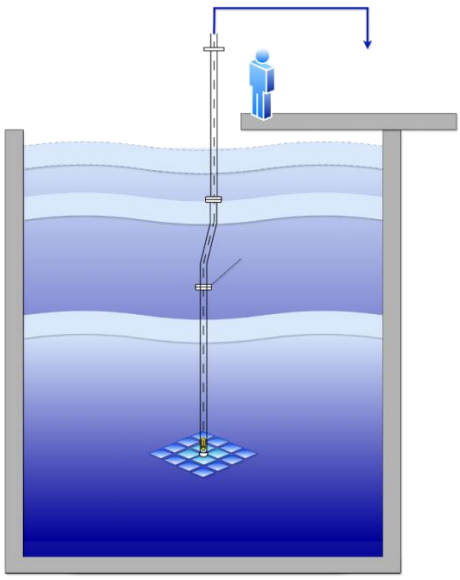

Fig. 9. Neutron flux measurement diagram.

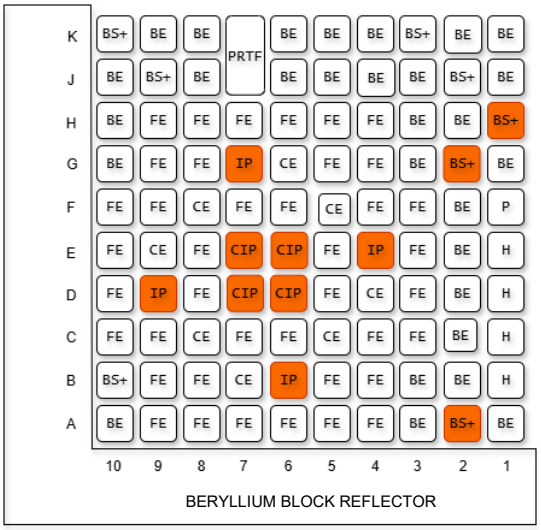

Fig. 10. Neutron flux measurement points.

Figure 10 shows the neutron flux measurement points in the RSG-GAS reactor core. Measurements at irradiation facilities were carried out both axially and radially at CIP positions (D6, D7, E6, E7), IP positions (B6, D9, E4, G7), and BS+ positions (A2, G2, H1).

In the neutron flux measurement using the SMFC CFUZ53 in current mode, an electric current is generated as the detector output due to the interaction between the neutron flux and the fissile material, which ionizes the gas inside the detector. This measured current will then be converted into the corresponding neutron flux value using Eq. (7). The SMFC CFUZ53, based on the specifications provided by the manufacturer, has a sensitivity value (S) of 5 x 10^{-18} A/n.cm^{-2}.s^{-1}.

$$\phi = \frac{I}{S} \tag{7}$$

where,

ϕ = Thermal neutron flux (n/cm^2.s)
I = Detector output current (A)
S = Detector sensitivity (A/n.cm^{-2}.s^{-1})

Neutron flux measurement using gold foil activation was carried out simultaneously with the SMFC CFUZ53 detector at the beryllium irradiation facility BS+ (positions A2, G2, H1). The thermal neutron flux measurement using the activation method involved two types of gold foils: a bare foil to detect both thermal and epithermal neutrons, and a cadmium-covered foil to detect only epithermal neutrons, as cadmium strongly absorbs thermal neutrons. By subtracting the activity of the cadmium-covered foil from that of the bare foil, the absolute thermal neutron flux (E < 0.5 eV) can be determined. In contrast,

the SMFC detector provides a relative neutron flux measurement. The ratio (r) between the absolute measurement from gold foil activation and the relative measurement from the SMFC detector is then calculated using Eq. (8). This ratio value (r) is then used as a correction factor for the neutron flux measurements obtained using the SMFC CFUZ53 detector, allowing for an accurate mapping of the neutron flux distribution within the RSG-GAS reactor core.

$$r = \frac{\phi_{gold\ foil\ activation}}{\phi_{detector}} \quad (8)$$

The results of all research activities will be analyzed in the form of neutron flux mapping using the SMFC CFUZ53 detector based on the manufacturer's sensitivity specification, analysis of gold foil activation results, and their comparison with the detector measurements to obtain a measurement ratio, and analysis of the corrected axial and radial neutron flux distribution at the irradiation facilities of the RSG-GAS reactor.

RESULTS AND DISCUSSION

Measurements analysis

The results of the gold foil activation process and neutron flux measurements using the detector at BS+ (A2, G2, and H1) produced the axial neutron flux distribution. Gold foil activation reference data for the Central Irradiation Position (CIP) and Irradiation Position (IP) were sourced from the 2024 RSG-GAS reactor neutron flux report (secondary data) acquired under identical reactor operating conditions. Single-point calibration values at CIP (E7) and IP (E4) served as normalization benchmarks to evaluate fission chamber measurements at adjacent irradiation positions at CIP (D6, D7, E6) and IP (B6, D9, G7).

Prior to reactor measurements, the SMFC CFUZ53 detector underwent comprehensive characterization, including operating voltage plateau testing, flux linearity verification, and dynamic response assessment. The detector exhibited ± 1.0% standard uncertainty determined via pre-operation current stability analysis. For gold foil activation, ± 3.0% uncertainty originated from gamma spectrum peak integration errors quantified using Genie2000 software. Propagating these independent uncertainties yielded a combined uncertainty of ± 4.0%.

Gold foil activation measurements at BS+ (A2, G2, H1), CIP (E7), and IP (E4) positions shared only one common axial elevation with detector measurements: 450 mm above the core base. To establish the systematic relationship between methods, fourth-degree polynomial regression was applied to determine relative deviations and calibration ratios across positions. Figs. 11-15 present gold foil activation data with regression curves ($R^2 > 0.94$) and SMFC CFUZ53 measurements acquired at 200 kW reactor power under consistent moderation conditions.

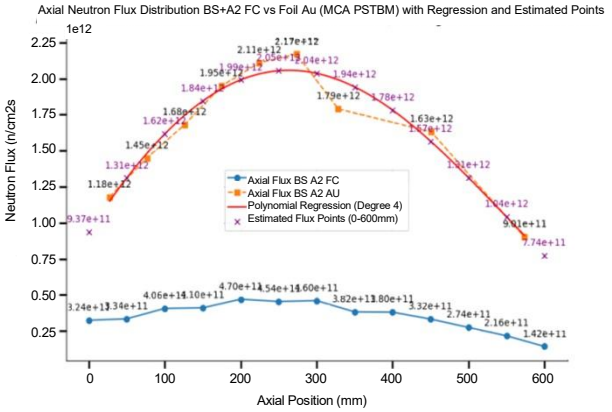

Fig. 11. Axial thermal neutron flux distribution at BS+ A2 (foil activation, regression, and detector).

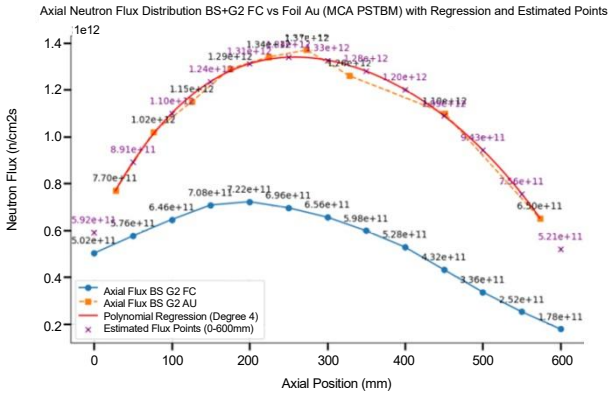

Fig. 12. Axial thermal neutron flux distribution at BS+ G2 (foil activation, regression, and detector).

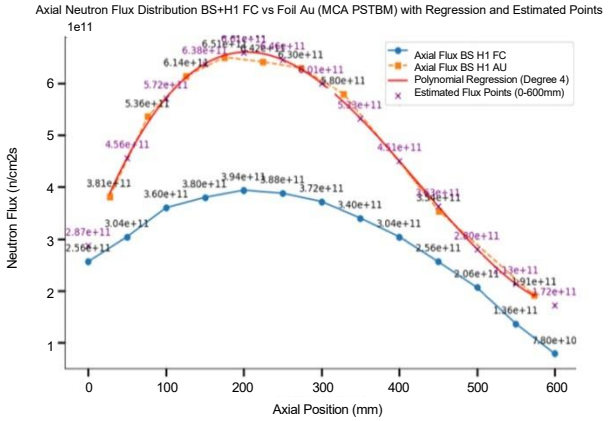

Fig. 13. Axial thermal neutron flux distribution at BS+ H1 (foil activation, regression, and detector).

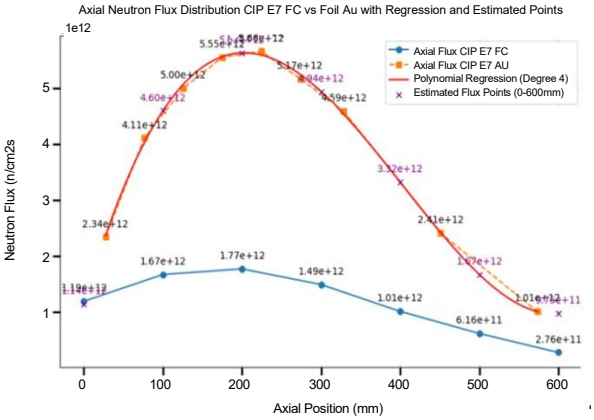

Fig. 14. Axial thermal neutron flux distribution at CIP E7 (foil activation, regression, and detector).

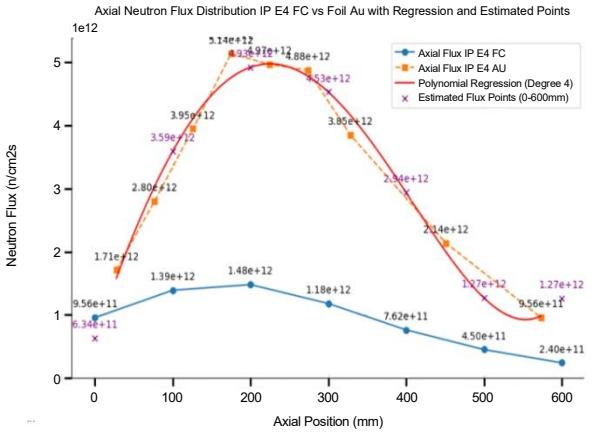

Fig. 15. Axial thermal neutron flux distribution at IP E4 (foil activation, regression, and detector).

Table 4. Relative deviation and measurement ratio of thermal neutron flux at BS+ A2.

Axial (mm)	Flux (x10^{12} n/cm^2.s)		Relative deviation (%)	Ratio
	SMFC CFUZ53	Gold Foil Regression		
0	0.324	0.937	- 65.422*	2.892
50	0.334	1.310	- 74.504	3.922
100	0.406	1.620	- 74.938	3.990
150	0.410	1.840	- 77.717	4.488
200	0.470	1.990	- 76.382	4.234
250	0.454	2.050	- 77.854	4.515
300	0.460	2.040	- 77.451	4.435
350	0.382	1.940	- 80.309	5.079
400	0.380	1.780	- 78.652	4.684
450	0.332	1.570	- 78.854	4.729
500	0.274	1.310	- 79.084	4.781
550	0.216	1.040	- 79.231	4.815
600	0.142	0.774	- 81.654	5.451

$$* \frac{(\phi_{fission\ chamber} - \phi_{gold\ foil\ activation})}{\phi_{gold\ foil\ activation}}\ x\ 100\%$$

Tables 4-8 present calculated relative deviations and measurement ratios derived from fourth-degree polynomial regressions of gold foil activation data at positions BS$^+$ (A2, G2, H1), CIP (E7), and IP (E4). The determination of the measurement ratio value is carried out for each measurement point because the detector response is influenced by the local neutron spectrum, which can vary along the axial axis due to differences in material structures, reflector effects, moderators, and coolant materials, as a function of flux density variations resulting from the reactor core geometry.

Table 5. Relative deviation and measurement ratio of thermal neutron flux at BS+ G2.

Axial (mm)	Flux (x10^{12} n/cm^2.s)		Relative deviation (%)	Ratio
	SMFC CFUZ53	Gold Foil Regression		
0	0.502	0.592	- 15.203	1.179
50	0.576	0.891	- 35.354	1.547
100	0.646	1.100	- 41.273	1.703
150	0.708	1.240	- 42.903	1.751
200	0.722	1.310	- 44.885	1.814
250	0.696	1.340	- 48.060	1.925
300	0.656	1.330	- 50.677	2.027
350	0.598	1.280	- 53.281	2.140
400	0.528	1.200	- 56.000	2.273
450	0.432	1.090	- 60.367	2.523
500	0.336	0.943	- 64.369	2.807
550	0.252	0.756	- 66.667	3.000
600	0.178	0.521	- 65.835	2.927

Table 6. Relative deviation and measurement ratio of thermal neutron flux at BS+ H1.

Axial (mm)	Flux (x10^{12} n/cm^2.s)		Relative deviation (%)	Ratio
	SMFC CFUZ53	Gold Foil Regression		
0	0.256	0.287	- 10.801	1.121
50	0.304	0.456	- 33.333	1.500
100	0.360	0.572	- 37.063	1.589
150	0.380	0.638	- 40.439	1.679
200	0.394	0.661	- 40.393	1.678
250	0.388	0.646	- 39.938	1.665
300	0.372	0.601	- 38.103	1.616
350	0.340	0.533	- 36.210	1.568
400	0.304	0.451	- 32.594	1.484
450	0.256	0.363	- 29.477	1.418
500	0.206	0.280	- 26.429	1.359
550	0.136	0.213	- 36.150	1.566
600	0.078	0.172	- 54.651	2.205

Table 7. Relative deviation and measurement ratio of thermal neutron flux at CIP E7.

Axial (mm)	Flux (x10^{12} n/cm^2.s)		Relative deviation (%)	Ratio
	SMFC CFUZ53	Gold Foil Regression		
0	1.194	-	-	-
100	1.670	4.600	- 63.696	2.754
200	1.772	5.630	- 68.526	3.177
300	1.494	4.940	- 69.757	3.307
400	1.008	3.320	- 69.639	3.294
500	0.616	1.670	- 63.114	2.711
600	0.276	0.970	- 71.546	3.514

Table 8. Relative deviation and measurement ratio of thermal neutron flux at IP E4.

Axial (mm)	Flux (x10^{12} n/cm^2.s)		Relative deviation (%)	Ratio
	SMFC CFUZ53 (x10^{12})	Gold Foil Regression (x10^{12})		
0	0.956	-	-	-
100	1.386	3.590	- 61.393	2.822
200	1.482	4.930	- 69.939	3.858
300	1.176	4.530	- 74.040	3.852
400	0.762	2.940	- 74.082	3.327
500	0.450	1.270	- 64.567	2.590
600	0.240	-	-	-

Table 9. Correction factor for neutron flux measurement.

Measuring points	Average ratio
BS+ A2	4.462
BS+ G2	2.125
BS+ H1	1.574
CIP E7	2.816
IP E4	3.290

Tables 4-8 demonstrate relative deviations exceeding 10% between gold foil activation and SMFC measurements, confirming that uncorrected detector readings lack sufficient accuracy for quantitative flux determination. Therefore, a correction factor in the form of a measurement ratio is required to adjust the neutron flux values obtained from the detector. The mean measurement ratios across BS+, CIP, and IP positions were applied as correction factors to the detector-derived neutron flux values, with comprehensive results detailed in Table 9. This ratio is used to convert the detector readings into an estimated absolute thermal neutron flux, enabling a more proper mapping of neutron flux at irradiation facilities within the RSG-GAS reactor core.

Using this correction factor, the corrected neutron flux distribution obtained from measurements using the SMFC CFUZ53 fission chamber detector is presented in Tables 10-13.

Table 10. Corrected axial thermal neutron flux distribution at CIP.

Points	Axial (mm)	Curr. (μA)	Flux (x10^{12} n/cm^2.s)		
			Actual	Corr.	Uncert.
CIP D6	0	3.960	0.792	2.233	±0.089
	100	5.890	1.178	3.322	±0.132
	200	6.670	1.334	3.762	±0.150
	300	5.740	1.148	3.237	±0.129
	400	4.000	0.800	2.256	±0.090
	500	2.510	0.502	1.416	±0.056
	600	1.550	0.310	0.874	±0.034
CIP D7	0	5.730	1.146	3.232	±0.129
	100	7.880	1.576	4.443	±0.177
	200	8.420	1.684	4.749	±0.190
	300	7.180	1.436	4.050	±0.162
	400	4.890	0.978	2.758	±0.110
	500	2.690	0.538	1.517	±0.060
	600	1.280	0.256	0.721	±0.028
CIP E6	0	4.880	0.976	2.752	±0.110
	100	7.230	1.446	4.078	±0.163
	200	7.900	1.580	4.456	±0.178
	300	6.860	1.372	3.869	±0.154
	400	4.720	0.944	2.662	±0.106
	500	2.930	0.586	1.653	±0.066
	600	1.610	0.322	0.908	±0.036
CIP E7	0	5.970	1.194	3.367	±0.134
	100	8.350	1.670	4.709	±0.188
	200	8.860	1.772	4.997	±0.199
	300	7.470	1.494	4.213	±0.168
	400	5.040	1.008	2.843	±0.113
	500	3.080	0.616	1.737	±0.069
	600	1.380	0.276	0.778	±0.031

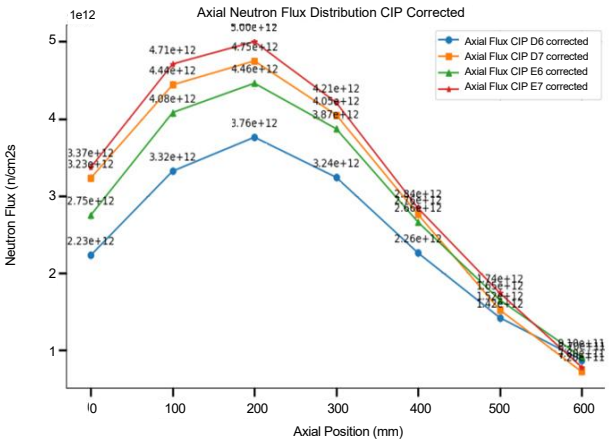

Fig. 16. Corrected axial thermal neutron flux distribution at CIP.

Table 10 presents the corrected axial neutron flux distribution ranging from 0 mm to 600 mm measured from the bottom of the reactor core at the CIP irradiation positions (D6, D7, E6, and E7). The data show that the highest axial flux occurs at 200 mm above the bottom of the core, with the highest average neutron flux recorded at CIP position E7, reaching 4.997 x 10^{12} ± 0.199 x 10^{12} n/cm².s. The neutron flux distribution at the CIP positions is illustrated in Fig. 16.

Table 11 presents the corrected axial neutron flux distribution from 0 mm to 600 mm above the bottom of the reactor core at the IP irradiation positions (B6, D9, E4, and G7). The data indicate that the highest axial flux occurs at 200 mm from the bottom of the core, with the highest average neutron flux observed at IP position B6, reaching 6.212 x 10^{12} ± 0.248 x 10^{12} n/cm².s. The neutron flux distribution at the IP positions is illustrated in Fig. 17.

Table 11. Corrected axial thermal neutron flux distribution at IP.

Points	Axial (mm)	Curr. (μA)	Flux (x10^{12} n/cm².s)		
			Actual	Corr.	Uncert.
IP B6	0	5.380	1.076	3.540	±0.141
	100	8.950	1.790	5.889	±0.235
	200	9.440	1.888	6.212	±0.248
	300	7.750	1.550	5.100	±0.204
	400	5.100	1.020	3.356	±0.134
	500	3.000	0.600	1.974	±0.078
	600	1.520	0.304	1.000	±0.040
IP D9	0	4.450	0.890	2.928	±0.117
	100	6.830	1.366	4.494	±0.179
	200	7.650	1.530	5.034	±0.201
	300	6.900	1.380	4.540	±0.181
	400	4.860	0.972	3.198	±0.127
	500	3.030	0.606	1.994	±0.079
	600	1.320	0.264	0.868	±0.034
IP E4	0	4.780	0.956	3.145	±0.125
	100	6.930	1.386	4.560	±0.182
	200	7.410	1.482	4.876	±0.195
	300	5.880	1.176	3.869	±0.154
	400	3.810	0.762	2.507	±0.100
	500	2.250	0.450	1.481	±0.059
	600	1.200	0.240	0.789	±0.031
IP G7	0	4.100	0.820	2.698	±0.107
	100	6.180	1.236	4.066	±0.162
	200	7.250	1.450	4.771	±0.190
	300	6.900	1.380	4.540	±0.181
	400	5.210	1.042	3.428	±0.137
	500	3.290	0.658	2.165	±0.086
	600	1.870	0.374	1.230	±0.049

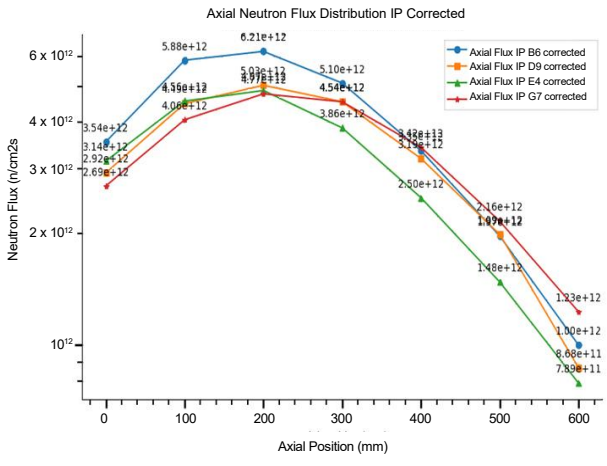

Fig. 17. Corrected axial thermal neutron flux distribution at IP.

Table 12 presents the corrected axial neutron flux distribution from 0 mm to 600 mm above the bottom of the reactor core at the BS+ irradiation positions (A2, G2, and H1). The data show that the highest axial flux occurs at 200 mm from the bottom of the core, with the highest average neutron flux measured at BS+ position A2, reaching 2.096 x 10^{12} ± 0.083 x 10^{12} n/cm².s. Although the BS+ irradiation positions are located outside the reactor core, the A2 position is closer to the reactor fuel elements, resulting in higher neutron flux measurements compared to the other positions (G2 and H1). The neutron flux distribution at the BS+ positions is illustrated in Fig. 18.

Table 12. Corrected axial thermal neutron flux distribution at BS+.

Points	Axial (mm)	Curr. (μA)	Flux (x10^{12} n/cm²s)		
			Actual	Corr.	Uncert.
BS+ A2	0	1.620	0.324	1.445	±0.057
	50	1.670	0.334	1.490	±0.059
	100	2.030	0.406	1.811	±0.072
	150	2.050	0.410	1.829	±0.073
	200	2.350	0.470	2.096	±0.083
	250	2.270	0.454	2.025	±0.080
	300	2.300	0.460	2.052	±0.082
	350	1.910	0.382	1.704	±0.068
	400	1.900	0.380	1.695	±0.067
	450	1.660	0.332	1.481	±0.059
	500	1.370	0.274	1.222	±0.048
	550	1.080	0.216	0.963	±0.038
	600	0.710	0.142	0.633	±0.025
BS+ G2	0	2.510	0.502	1.064	±0.042
	50	2.880	0.576	1.221	±0.048
	100	3.230	0.646	1.370	±0.054
	150	3.540	0.708	1.501	±0.060
	200	3.610	0.722	1.531	±0.061
	250	3.480	0.696	1.476	±0.059
	300	3.280	0.656	1.391	±0.055
	350	2.990	0.598	1.268	±0.050
	400	2.640	0.528	1.119	±0.044
	450	2.160	0.432	0.915	±0.036
	500	1.680	0.336	0.712	±0.028
	550	1.260	0.252	0.534	±0.021
	600	0.890	0.178	0.377	±0.015
BS+ H1	0	1.280	0.256	0.401	±0.016
	50	1.520	0.304	0.477	±0.019
	100	1.800	0.360	0.565	±0.022
	150	1.900	0.380	0.596	±0.023
	200	1.970	0.394	0.618	±0.024
	250	1.940	0.388	0.609	±0.024
	300	1.860	0.372	0.584	±0.023
	350	1.700	0.340	0.533	±0.021
	400	1.520	0.304	0.477	±0.019
	450	1.280	0.256	0.401	±0.016
	500	1.030	0.206	0.323	±0.012
	550	0.680	0.136	0.213	±0.008
	600	0.390	0.078	0.122	±0.005

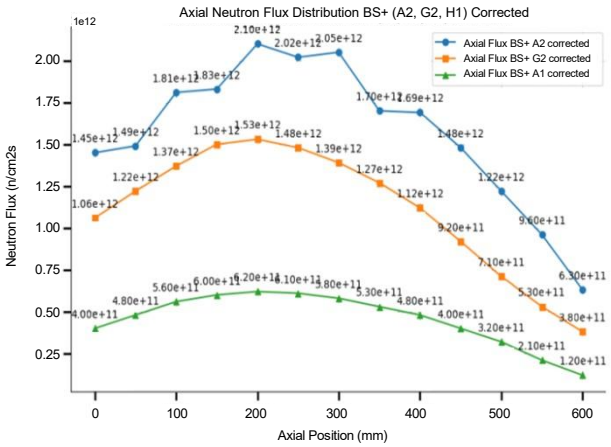

Fig. 18. Corrected axial thermal neutron flux distribution at BS+.

Table 13. Radial neutron flux distribution.

Points	Current (μA)	Flux (x10^{12} n/cm^{2}s)		
		Actual	Corr.	Uncert.
CIP D6	1.550	0.310	0.874	±0.034
CIP D7	1.280	0.256	0.721	±0.028
CIP E6	1.610	0.322	0.908	±0.036
CIP E7	1.380	0.276	0.778	±0.031
IP B6	1.520	0.304	1.000	±0.040
IP D9	1.320	0.264	0.868	±0.034
IP E4	1.200	0.240	0.789	±0.031
IP G7	1.870	0.374	1.230	±0.049
BS+ A2	0.710	0.142	0.633	±0.025
BS+ G2	0.890	0.178	0.377	±0.015
BS+ H1	0.390	0.078	0.122	±0.005

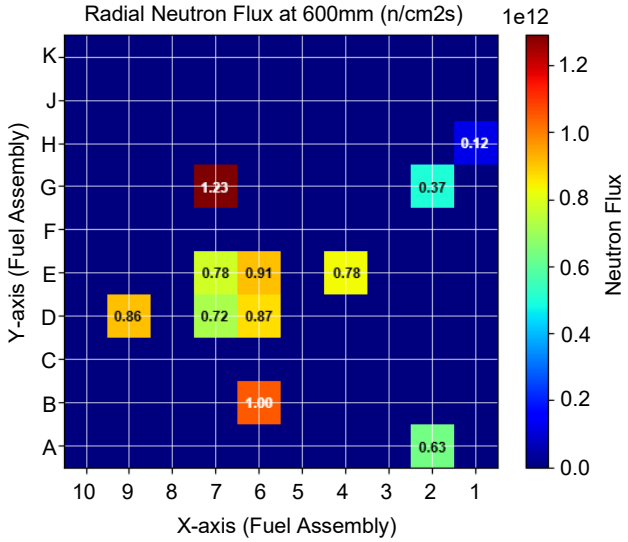

Fig. 19. Radial neutron flux mapping.

Table 13 presents the corrected radial neutron flux distribution at 600 mm above the core base (top core elevation) in the RSG-GAS reactor. The results reveal a peak thermal neutron flux of 1.230 x 10^{12} ± 0.049 x 10^{12} n/cm^2.s at irradiation position IP-G7, consistent with the reactor's radial power profile.

These measurements were used to generate the flux mapping shown in Fig. 19, which visually highlights the spatial flux gradient across the core.

Comparison with previous studies

Neutron flux measurements at the RSG-GAS reactor have predominantly utilized the foil activation method. Several studies have benchmarked these experimental results against computational models. Notably, comparisons between experimental data and MCNP simulations have demonstrated close agreement, with discrepancies of approximately 2%. In contrast, calculations performed using the Batan-3DIFF program exhibited a larger average deviation of 7% [28]. Further advancements in measurement techniques have incorporated beta-gamma coincidence systems alongside gamma spectrometry, achieving a higher precision with differences reduced to around 1.5% [29]. To further enhance the measurement accuracy, specific correction factors, including self-shielding effects, have been rigorously investigated [30]. In contrast to prior research at the RSG-GAS reactor, which relied predominantly on activation techniques, this study presents the first systematic benchmarking of in-core neutron flux measurements, directly comparing Sub-Miniature Fission Chamber (SMFC) results against the conventional foil activation method. The findings validate the SMFC's reliability and demonstrate its significant potential for real-time, in-core neutron flux monitoring in mixed-spectrum research reactors. In this work, an average correction factor was applied for the CIP positions based on the assumption that the nearby CIP locations have similar neutron spectra. Since detailed spectral measurements at each CIP were not available, this assumption has to be verified by additional foil activation or spectral comparison in future work if higher accuracy is required.

CONCLUSION

This study demonstrates the application of a Sub-Miniature Fission Chamber (SMFC) for neutron flux monitoring in the RSG-GAS research reactor. The primary objective was to validate the SMFC's performance by benchmarking its measurements against the conventional gold foil activation method, establishing it as a reliable and efficient alternative for in-core flux mapping. The SMFC CFUZ53 detector successfully mapped neutron flux distributions in the RSG-GAS reactor core, measuring peak axial fluxes of 6.212 x 10^{12} ± 0.248 x 10^{12} n/cm^2.s (IP B6),

4.997 x 10^{12} ± 0.199 x 10^{12} n/cm².s (CIP E7), and 2.096 x 10^{12} ± 0.083 x 10^{12} n/cm².s (BS+ A2) at 200 mm elevation, with a radial maximum of 1.230 x 10^{12} ± 0.049 x 10^{12} n/cm².s at IP G7 (600 mm elevation). Data from measuring positions at BS+/CIP/IP were corrected using gold foil activation, demonstrating the detector's capability to provide rapid, high-resolution flux measurements while reducing uncertainty compared to conventional activation methods. These results establish fission chambers as a viable alternative for in-core neutron monitoring for the RSG-GAS reactor. For future research, the influence of the detector guide tube assembly on the sub-miniature fission chamber's response will be characterized to quantify its impact on measurement accuracy. Furthermore, the fission chamber will be recalibrated across a range of operational regimes including varying power levels and fuel cycles to establish robust correction factors and ensure consistent, reproducible flux measurements across all core positions and throughout the reactor's operating cycle. The use of an average correction factor for CIP positions is valid only if the nearby positions have similar neutron spectra, which should be verified in future work.

ACKNOWLEDGMENT

The authors gratefully acknowledge the financial support from the National Research and Innovation Agency (BRIN) through the Degree by Research scholarship, which enabled the completion of this master's research in Engineering Physics at Universitas Gadjah Mada (UGM). Special thanks are extended to the Nuclear Reactor Technology Research Center and PT. Halia Teknologi Nusantara for providing technical resources essential for this study. This work forms part of the first author's thesis, and its successful execution owes much to these institutions' collective support.

AUTHOR CONTRIBUTION

Ranji Gusman led the research design, methodology development, data collection and analysis, and manuscript drafting as first author. Alexander Agung supervised the project, validated findings, and edited the manuscript as the corresponding author. R. Mohammad Subekti provided technical supervision and verified the analytical methods. Fauzi Nur Iswahyudi and Fitri Susanti conducted the experimental neutron flux measurements using both SMFC detectors and foil activation techniques. Surian Pinem contributed to the nuclear physics theoretical framework and discussion sections.

REFERENCES

1. S. Pinem, P. H. Liem, F. Susanti *et al*., Ann. Nucl. Energy **213** (2025) 1.
2. M. T. Aitkulov, D. S. Dyussambayev, N. K. Romanova *et al*., J. Phys.: Conf. Ser. **2155** (2022) 1.
3. S. Pinem and T. M. Sembiring, Int. J. Nucl. Energy Sci. Technol. **13** (2019) 295.
4. R. S. A. Kuswandrata, A. Agung, S. Syarip *et al*., *Performance Test of SPND Neutron Detector and Neutron Flux Mapping of Kartini Reactor Corein*, in: AIP Conference Proceeding (2024) 130006-1.
5. R. S. A. Kuswandrata, A. Agung, A. R. Antariksawan *et al*., Jurnal Sains dan Teknologi Nuklir Indonesia **25** (2024) 44. (in Indonesian)
6. W. Karsono, A. Agung, and A. R. Antariksawan *et al.*, Jurnal Sains dan Teknologi Nuklir Indonesia **25** (2024) 20. (in Indonesian)
7. L. Barbot, C. Domergue, J-F. Villard e*t al., On Line Neutron Flux Mapping in Fuel Coolant Channels of a Research Reactor,* in: 3rd International Conference on Advancements in Nuclear Instrumentation, Measurement Methods and Their Applications (ANIMMA), IEEE (Institute of Electrical and Electronics Engineers), Marseille (2013) 1.
8. O. Poujade and A. Lebrun, Nucl. Instrum. Methods. Phys. Res. A **433** (1999) 673.
9. K. R. Prasad and V. Balagi, Rev. Sci. Instrum. **67** (1996) 2197.
10. Z-P. Wu, X. -B. Jiang, W-S. Zhang *et al*., Nucl. Sci. Tech. **33** (2022) 78.
11. P. H. Liem and T. M. Sembiring, Nucl. Eng. Des. **240** (2010) 1433.
12. T. M. Sembiring, Tukiran, and S. Pinem, Atom Indones. **27** (2001) 85.
13. RSG-Badan Tenaga Nuklir Nasional (BATAN), Multipurpose Reactor G.A. Siwabessy Safety Analysis Report. Rev. 10, BATAN, Jakarta (2011).
14. S. Pinem, W. Luthfi, P. H Liem *et al*., Nucl. Eng. Technol. **55** (2023) 1775.
15. S. Pinem, T. M. Sembiring, and P. H. Liem, Atom Indones. **42** (2016) 123.
16. S. Pinem, J. Susilo, Tukiran *et al.*, Teknologi Indonesia **35** (2012) 37.
17. G. de Izarra, EPJ Nuclear Sci. Technol. **6** (2020) 1.

18. A. Antolínez and D. Rapisarda, Nucl. Instrum. Methods Phys. Res. A **825** (2016) 6.

19. L. Oriol, C. Blandin, S. Bréaud *et al*., *In-pile CFUZ53 Sub-Miniature Fission Chambers Qualification in BR2 Under PWR Conditions*, in: 10th International Group on Research Reactors (IGORR-10) Meeting (2005) 1.

20. M. A. Reichenberger, T. C. Unruh, P. B. Ugorowski *et al*., Ann. Nucl. Energy **87** (2016) 318.

21. J. Coburn, S. M. Luker, E. J. Parma *et al.*, *Modeling, Calibration, and Verification of a Fission Chamber for ACRR Experimenters,* in: EPJ Web Conf, EDP Sciences (2016) 05001-p.1.

22. E. Teimoory, M. A. Allaf, J. Mokhtari *et al.*, Radiat. Phys. Chem. **215** (2024) 1.

23. B. Geslot , F. Berhouet, L. Oriol *et al*., *Development and Manufacturing of Special Fission Chambers for In-core Measurement Requirements in Nuclear Reactors* in: Proceedings of the 1st International Conference on Advancements in Nuclear Instrumentation, Measurement Methods and their Applications (ANIMMA), EDP Sciences, Les Ulis (2009) 1.

24. S. P. Chabod, Nucl. Instrum. Methods Phys. Res. A **598** (2009) 578.

25. A. B. di Tigliole, A. Cammi D. Chiesa *et al*., Prog. Nucl. Energy **70** (2014) 249.

26. T. Kimeridze and T. C. H. Nguyen, Georg. Sci. **5** (2023) 189.

27. International Atomic Energy Agency (IAEA), Neutron Fluence Measurements, Technical Reports Series No. 107, IAEA, Vienna (1970).

28. S. Pinem and T. M. Sembiring, Int. J. Nuclear Energy Sci. Technol. **13** (2019) 295.

29. S. Bakhri, *Sistem Deteksi Radiasi Koinsiden untuk Penentuan Fluks Neutron Termal Fasilitas Iradiasi Reaktor Penelitian RSG-GAS*, in: Prosiding Seminar Hasil Penelitian P2TRR, P2TRR - BATAN (2002) 25. (in Indonesian)

30. B. Radiyanti, A. Hamzah., and S. Pinem *et al*., *Analisis Faktor Koreksi Keping Aktivasi dan Pengaruh Pengabaiannya pada Pengukuran Fluks dan Spektrum Neutron,* in: Pertemuan dan Presentasi Ilmiah Penelitian Dasar Ilmu Pengetahuan Teknologi Nuklir (1996) 194. (in Indonesian)